Soft Matter

Accepted Manuscript

ROYAL SOCIETY OF CHEMISTRY

www.rsc.org/softmatter

ARTICLE TYPE www. rsc.org/xxxxxx | XXXXXXXX

Transverse migration of polyelectrolytes in microfluidic channels induced by combined shear and electric fields

Mert Arca, Jason E. Butler and Anthony J. C. Ladd*

Received Xth XXXXXXXXXX 20XX, Accepted Xth XXXXXXXXX 20XX
First published on the web Xth XXXXXXXXXX 200X
DOI: 10.1039/b000000x

If a dilute solution of a polyelectrolyte such as DNA is forced through a microcapillary by an electric field, while simultaneously driven by a pressure gradient, then the polymer will migrate in directions transverse to the field lines. Here we investigate the sharp increase in concentration in the center of the channel that arises when the flow and electric field drive the polymer in the same direction. We report the first systematic investigation of the effects of flow velocity, electric field, and ionic strength on the degree of migration. We find that migration increases with increasing shear and electric field as predicted by kinetic theory [Butler *et. al Phys. Fluids*, 2007, **19** 113101], but eventually saturates as suggested by computer simulations [Kekre *et. al Phys. Rev. E*, 2010, **82** 050803(R)]. The addition of salt reduces the strength of the migration, consistent with a screening of long-range hydrodynamic flow fields by added salt. However, increasing the ionic strength of a tris-acetate-EDTA buffer solution has much less effect on the degree of migration.

1 Introduction

Although there is an extensive literature on the interactions of polyelectrolytes with electric fields[1,2] and of polymers with a shear flow[3,4], much less is known about the combined effects of these fields on charged polymers. If a polyelectrolyte undergoing capillary electrophoresis is subjected to a simultaneous pressure gradient, it will migrate in a direction perpendicular to the field lines[5,6]. The migration is an effect of the flow and electric fields acting in tandem, and vanishes when either field is removed[5]. It was proposed[7] that this migration is due to an electrically induced hydrodynamic interaction (EIHI); the mechanism is illustrated in Fig. 1.

A polymer can be modeled as a chain of blobs, with an excluded volume interaction between each blob; in the case of a charged polymer the blob is electrically neutral but the charge distribution is polarizable. In the presence of an electric field perturbations in the charge distribution generate a disturbance in the flow[8], which at large distances decays as $1/r^3$, where r is the distance from the center of the blob. Although a blob of polyelectrolyte (including counterions) is electrically neutral, there is still this long-range dipolar flow around the ion when it is subjected to an electric field[8,9]

$$\vec{u}(\vec{r}) = \frac{\lambda_D^2}{4\pi\mu r^3}\left(\frac{3\vec{r}\vec{r}}{r^2} - 1\right)\cdot Q\vec{E}, \qquad (1)$$

where λ_D is the Debye screening length, Q is the total charge on a blob, and μ is the solvent viscosity. The flow field around each blob is a double-vortex, as shown schematically in Fig. 1. Equation (1) is the limiting case when the Debye length is much larger than the ion size. It is the size of the individual charged segments (< 1 nm) that is the relevant scale here, not the size of the blob[9].

The electrically-induced flow around a polyelectrolyte blob induces a force on a neighboring blob so that it translates with

Department of Chemical Engineering, University of Florida, Gainesville, Florida 32611, USA ; Tel:352-392-6509; E-mail:tladd@che.ufl.edu

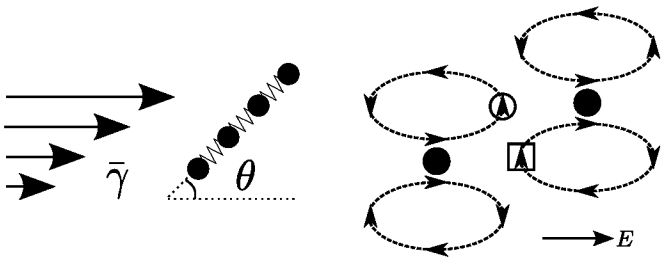

Fig. 1 Migration of a polyelectrolyte in combined shear and electric fields. A pressure driven flow in the microchannel generates a spatially varying shear rate (zero at the channel center, maximum near the wall, average $\bar{\gamma}$), which stretches and orients the polymer at a mean angle θ to the flow direction, lying in the first quadrant. The polymer can be thought of as a chain of connected blobs (filled circles), each blob representing short segments of DNA, which repels other blobs due to steric repulsion between the segments. The blobs contain the charged DNA backbone and corresponding counter ions. An electric field applied to a (polarizable) blob generates a dipolar flow around it, as indicated in the sketch (far right). The flow field around the first (left) blob generates its maximum transverse velocity (circled arrow) along the 45° direction. This causes a net lift to the neighboring blob which exerts a similar effect on the first blob (square). Thus, when the flow and electric fields are concurrent, the polyelectrolyte drifts towards the center of the channel; when they act in opposition, the mean orientation is in the second quadrant and the polyelectrolyte drifts towards the wall[7].

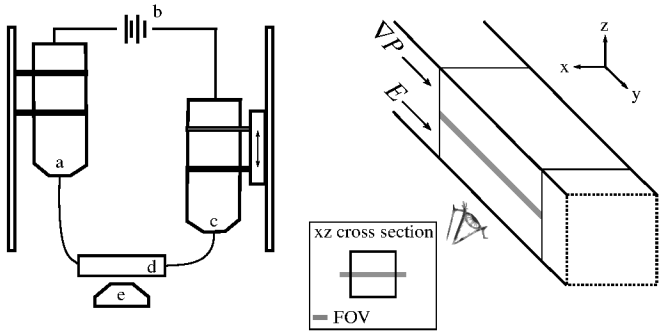

Fig. 2 Schematic diagram of the experiment. In the left panel, the arrangement of the key components is indicated: (a) fixed reservoir, (b) voltage generator, (c) adjustable reservoir, (d) microfluidic channel, and (e) objective. A three-dimensional view of the microfluidic channel is shown on the right, with the imaging region (about 200 μm on a side) shaded. Center: Cross section of the device with the field of view (FOV) shaded.

respect to the local stream velocity; the direction of the force depends on the orientation of the vector between the blobs. On average, the forces from an isotropic distribution of neighboring blobs will cancel and a discernible effect therefore depends on the polymer being stretched, typically by a shear flow, as well as being subjected to an electric field; a typical experimental realization is illustrated in Fig. 2. A pressure-driven flow in the capillary induces a stretching of the polymer (for sufficiently large flow rates), which then aligns itself on average in the first quadrant[10], as shown in Fig. 1. In this configuration, the electrically-induced flow field from the left bead pushes the right bead upward (as indicated by the circled arrow), while the right bead pulls the left bead upward as well (square). Thus a pair of blobs, driven to the first quadrant by the shear, migrate towards the center of the channel when the electric field drives the polymer in the same direction as the flow, while if the flow and electric fields are in opposition the polymer migrates towards the wall[7]. With a combination of flow and electric field it is then possible to control the concentration of a polyelectrolyte in a micro capillary. More generally, the mechanism sketched in Fig. 1 suggests that the electrophoretic mobility of DNA is configuration dependent[8]. For example, during electrophoresis in a narrow and converging channel, a polyelectrolyte is stretched and forced to align with the field ($\theta \approx 0$ in Fig. 1), which leads to a length-dependent enhancement of the electrophorectic mobility[11].

Polyelectrolyte migration has been studied theoretically by applying kinetic theory to a dumbbell model of the polymer[12]. The theory predicts that, when the flow and electric fields are aligned (as illustrated in Fig. 1), the polyelectrolyte concentration is Gaussian-distributed about the center of the channel, with a width σ that scales with the flow rate and electric field as

$$\frac{R_G}{\sigma} = C\sqrt{\frac{WiWi^E\lambda_D}{h}}, \qquad (2)$$

where h is the channel width (80 μm in these experiments), R_G is the radius of gyration of the polymer ($R_G = 0.75\,\mu$m for λ–DNA) and C is a constant. Here we have characterized the flow and electric field in terms of two dimensionless Weissenberg numbers:

$$Wi = \bar{\gamma}\tau \quad \text{and} \quad Wi^E = \mu^E E \tau / R_G. \tag{3}$$

The mean shear rate in a channel flow is taken as $\bar{\gamma} = 2v_0/h$ where v_0 is the fluid velocity at the centerline and is proportional to the height difference between the two reservoirs (Fig. 2); τ is taken as the viscous relaxation time[13], which for λ–DNA in water is $\tau = 0.1\,$s[14]. We used Manning's theory[15] for the electrophoretic mobility μ^E to convert from electric field to Weissenburg number $Wi^E = \mu^E E\tau/R_G$; the values are given in Table 1. In Sec. 4.2 we report experimental tests of the predicted scaling with shear rate and electric field.

Brownian dynamics simulations of polyelectrolytes in shear and electric fields[9] found concentration profiles in quantitative agreement with experimental measurements[5], but predicted a saturation in the migration with increasing electric field. The experimental work reported in this paper was designed to test this prediction. Since the polymer velocities (in excess of 100 μm s^{-1}) are too large for direct imaging of the DNA, we have determined the average concentration field from the distribution of fluorescence intensity across the channel. We report the first systematic experimental investigation of the effects of flow, electric field, and ionic strength on polyelectrolyte migration. The experimental set-up is described in Sec. 2 and the image processing in Sec. 3; results are presented in Sec. 4 followed by the conclusions (Sec. 5).

Table 1 Solution properties. The compositions of the solutions are given in mM and the Debye length is in nm; the electrophoretic mobility is in units of μm s^{-1}(V/cm)$^{-1}$. The corresponding data for the simulations[9] are also shown.

Solution	TAE	NaCl	I	λ_D	μ^E
S1	40	0	7.3	3.6	5.0
S2	0.4	0.1	0.17	23.3	6.7
S3	0.4	0.25	0.32	17.1	6.4
S4	0.4	2.5	2.6	6.0	5.5
Simulation	0	0.005	0.005	140	7.85

2 Experimental Methods

Concentrations of fluorescent DNA molecules in a microfluidic channel were captured using optical microscopy. Molecules of λ-DNA (48,502 base pairs, New England BioLabs) were labeled with YOYO-1 (Molecular Probes) with a ratio of 5 base pairs to 1 dye molecule[16]. An 0.1 pM solution of labeled DNA was prepared in a Tris-acetate-EDTA (TAE) buffer (Sigma Aldrich) with two different concentrations; the standard 40 mM buffer solution (1×TAE) and a reduced strength 0.4 mM TAE solution (0.01×TAE); both buffers have a pH of 8.3. The ionic strength of the solution was adjusted by adding NaCl to the reduced strength 0.01×TAE solution. The compositions of the solutions are reported in Table 1.

The prepared solution was distributed between two 50 ml reservoirs, 20 ml to each reservoir. Electric fields up to 5 V (DC) were generated (Agilent 3321A) and amplified 200 fold (Trek 2220) to a maximum of 1 kV. Flow in the microchannel was introduced by placing the reservoirs at slightly different heights, using a computer-controlled translation stage (Thorlabs) to produce an accurate height difference. The distribution of fluorescent markers were imaged in a single viewing plane with a Nikon Diaphot 200 inverted microscope equipped with a QImaging Retiga SRV CCD camera and Leitz Wetzlar

(63x) objective. A schematic drawing of the experimental layout is shown in Fig. 2.

Straight silica microchannels with inner dimensions $80 \times 80\,\mu$m (Wale Apparatus) were embedded in PDMS (Slygard 184 silicone elastomer kit) during the hardening process[17]. Images were recorded within a $200\,\mu$m window, placed about 25 mm from the entrance of a 42 mm long channel to minimize perturbations from the fluid entering the capillary. The fluorescence intensity was recorded for approximately 5 minutes in each experiment.

Single particle tracking[18,19] was used the calibrate the fluid velocity at the center of the channel with the height difference of the reservoirs. The average shear rate $\bar{\gamma}$ can then be obtained from the centerline velocity v_0; $\bar{\gamma} = 2v_0/h$, where $h = 80\,\mu$m is the width of the channel. The calibration was performed at lower velocities than are required to generate significant migration; the appropriate height difference was subsequently obtained by extrapolation, assuming a linear relation between velocity and height difference.

3 Image Processing

Images were captured every 100 ms over a period of approximately 5 minutes, using Nikon Elements software, and then converted to AVI format for processing within MATLAB®. For shear rates sufficient to cause migration, the flow velocity is too fast ($> 100\,\mu\mathrm{m\,s^{-1}}$) to allow for direct imaging and tracking of the DNA. Instead we capture a time-averaged concentration field by accumulating the intensities of the individual frames, which results in a significantly enhanced signal-to-noise ratio. Examples of the accumulated intensity, normalized by the number of frames, are shown in the first row of Fig. 3 for three different electric fields. The raw images show migration of the DNA towards the center of the channel, as indicated by the enhanced fluorescence intensity, which is largest for the intermediate field ($19\ \mathrm{V\,cm^{-1}}$). The quality of the image can be enhanced by normalizing, pixel-by-pixel, with a background image obtained at zero electric field, which eliminates most of the artifacts of the optical system. This assumes a localized but non-uniform response of the optical system to a fluorescent source, $I(r) = \int F(r,r')c(r')dr'$, where $c(r)$ is the local concentration, and the instrument function $F(r,r') = F(r)\delta(r-r')$. In the absence of an electric field we expect no measurable migration in a channel that is much larger than the radius of gyration of the DNA[5], which is confirmed by the almost uniform distribution in the normalized intensity at $1\mathrm{V\,cm^{-1}}$ (Fig. 3d). We have verified that images with non-zero electric field and zero flow rate are indistinguishable from images at finite flow rate and zero electric field. However, it is generally more convenient to fix the flow rate and vary the electric field, so the intensity distribution at zero electric field was used to normalize all the data at a single flow rate. Images of the normalized concentration fields are shown in the second row of Fig. 3.

The variation in concentration across the channel (left to right) can be obtained with higher precision by integrating the intensities over the length of the viewing window (top to bottom). This gives the concentration profiles shown in the third row of Fig. 3. The data in Fig. 3h is reproduced in Fig. 4 to indicate the characterization of the concentration field by its amplitude and width.

The amplitude of the concentration profile was taken as the difference between the maximum and minimum values across

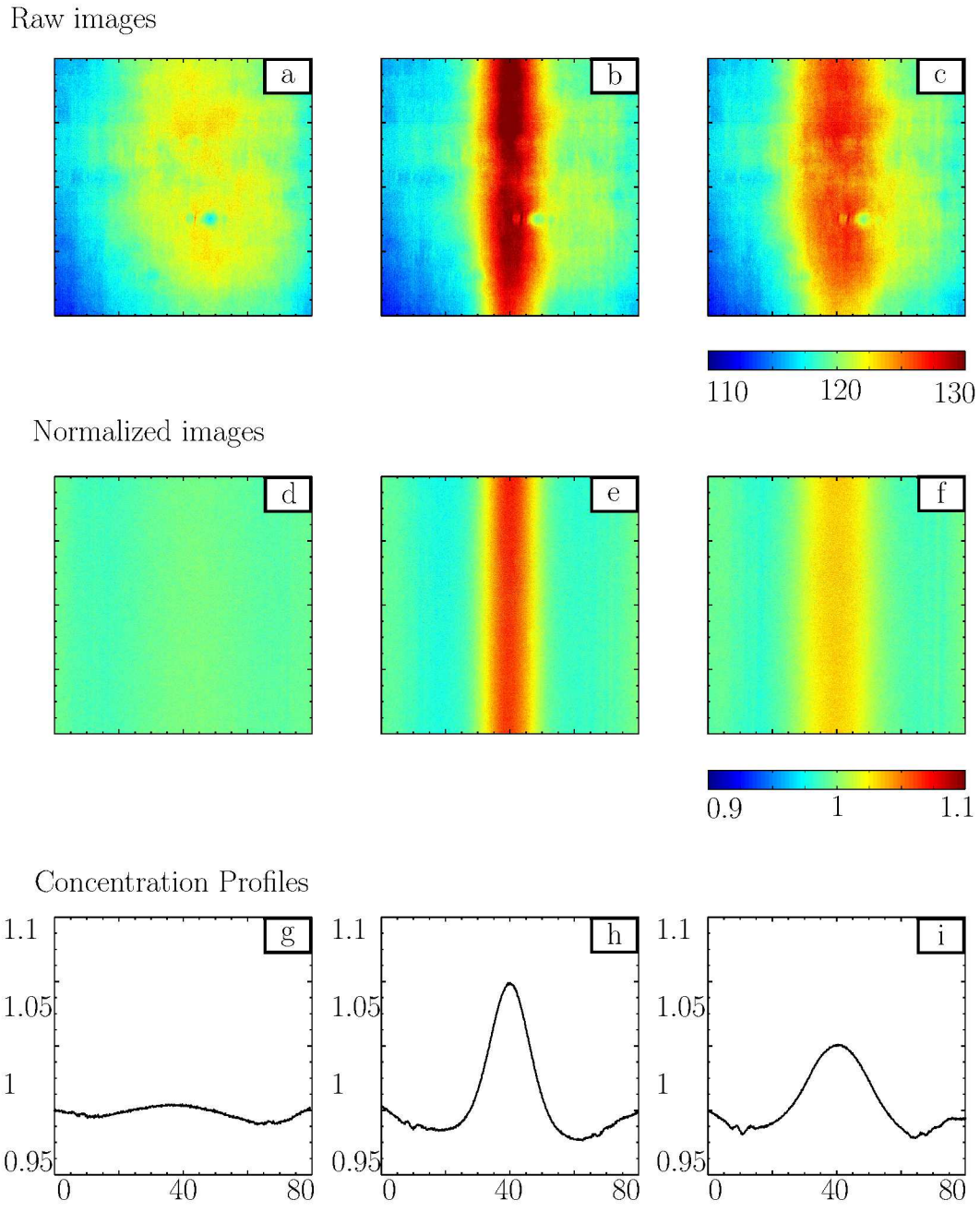

Fig. 3 Examples (solution S2 at $Wi = 0.6$) of the fluorescence intensity, integrated over a time of approximately 5 minutes. Panels (a–c) are raw two dimensional images, obtained with electric fields of 1, 19 and 238 $\mathrm{V\,cm^{-1}}$ respectively. Panels (d–f) are the same images normalized by a background field with a flow rate only ($E = 0$). Panels (g–i) are the profiles obtained by averaging the data shown in panels (d–f) over the flow direction (top to bottom).

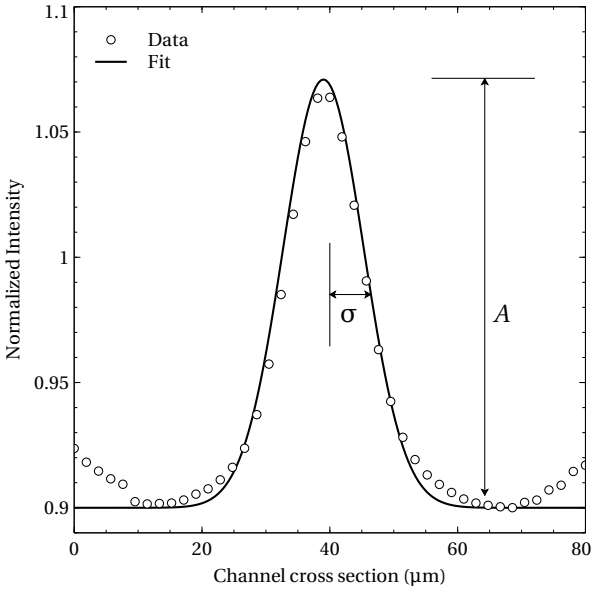

Fig. 4 Fitting of a typical intensity profile. The experimental data (open circles) from Fig. 3h (solution S2, $Wi = 0.6$, $E = 19\ V/\mathrm{cm}$) is fitted to a Gaussian function $A\exp[-(x-40)^2/2\sigma^2]$ in the region near the maximum in the intensity. The amplitude A and width σ are subsequently used to characterize the intensity profile.

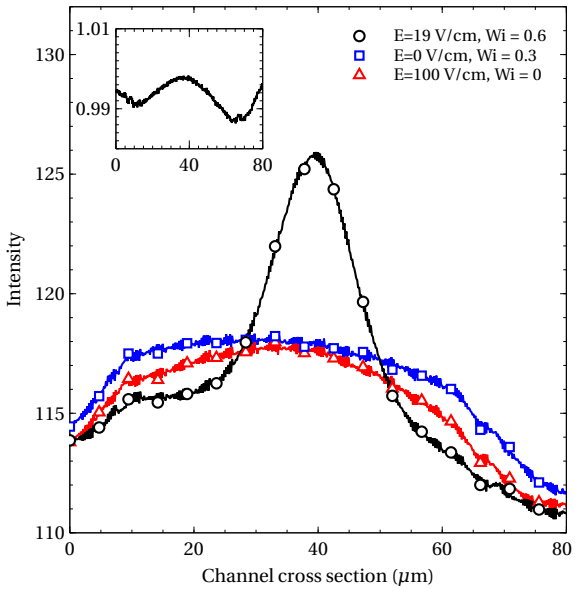

Fig. 5 Distribution of fluorescence intensity across the channel. Raw data was integrated over time and over the length of the viewing window: Combined flow and electric fields (black circles); pressure-driven flow only (blue squares); electric field only (red triangles). The inset shows the ratio of the background intensities (red/blue); note the enhanced scale.

the channel (Fig. 4). The scale for the amplitude is not arbitrary, but reflects the fluorescence intensity relative to the mean intensity of the background image. The extent of migration is reflected by the width of the concentration distribution as well as the amplitude; the width is of additional interest because it can be predicted by kinetic theory[12] as well as by numerical simulations[9].

The intensity in Fig. 4 shows a statistically significant increase near the channel walls when normalized by the background signal from either a pressure driven flow (with zero field) or an electric field (with zero flow). The raw fluorescence intensity, integrated along the length of the viewing window and over time is shown in Fig. 5. There is a significant decrease in intensity near the channel walls even for the background images where there should be next to no migration. We believe this is an imaging artifact, caused by the proximity of the glass walls; the asymmetry in the signal is due to a slight misalignment of the channel in the PDMS base. Our most reliable data is then limited to the center region of the channel, from $20\,\mu$m to $60\,\mu$m where the instrument response is nearly linear (see inset to Fig. 5). We therefore fit a Gaussian distribution to the normalized intensity data in the center of the channel ($20-60\,\mu$m),

$$I(x) = \frac{1}{\sqrt{2\pi\sigma^2}}\exp^{(x-h/2)^2/2\sigma^2}, \qquad (4)$$

using the nonlinear least squares method.

4 Results

Using the methods described in the previous sections, we have analyzed the results of a number of experiments, characteriz-

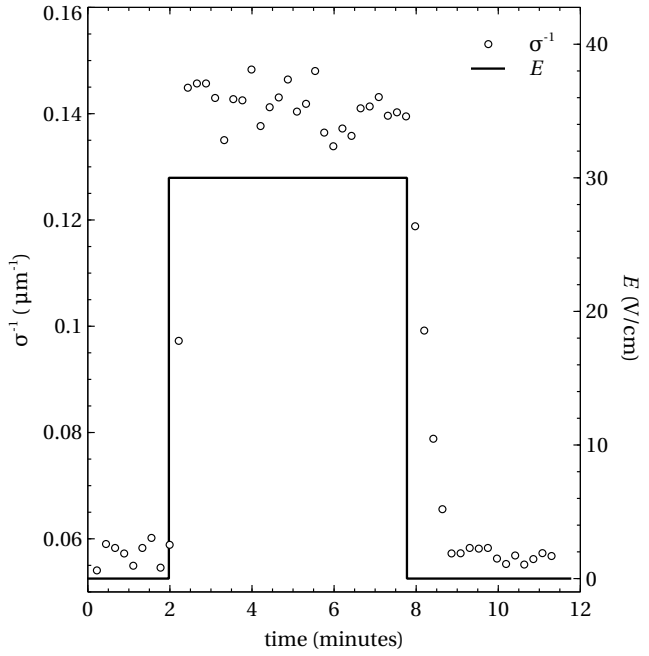

Fig. 6 Transient migration in a time varying electric field (solution S2, $Wi = 0.6$). Before the electric field is applied, at $t = 2$ minutes, the solution is fully mixed as indicated by the small value of σ^{-1}. After the electric field is applied, the DNA solution reaches a de-mixed state characterized by a narrow profile (see Fig. 4), as indicated by the sharp increase in σ^{-1} within $15-30$ s. Once the electric field is turned off (at 8 minutes), it takes about one minute for a new solution to replace the de-mixed DNA in the field of view.

ing the distribution of fluorescence intensity across the channel (as a marker for concentration) in terms of its amplitude and width (Fig 4). We have investigated the dependence of the (steady-state) concentration distribution of DNA on flow rate, electric field, and ionic strength, and also its transient response to a pulsed DC field.

4.1 Migration of DNA in a pulsed electric field

Transient experiments were conducted by pulsing a DC electric field of 30 V/cm every 6 minutes. The flow rate was kept constant, with a Weissenberg number $Wi = 0.6$; at this shear rate the polymer is elongated and rotated by the shear but not yet fully extended[14]. Figure 6 shows measurements of the inverse width over one representative cycle of the electric field; typical experiments include many such cycles with essentially identical results from each cycle. Images were recorded at 2.5 cm from the inlet of a 4.2 cm long channel, which is sufficiently far from the inlet (over 300 times the channel width) to eliminate entrance effects. Data was collected every 13.5 s, averaging over 150 frames with an exposure of 90 ms per frame.

Before applying the electric field ($t < 2$ min), the inverse width was low, indicating that the solution was fully mixed. In the absence of a significant concentration profile, the fitting procedure gives a finite value, related to the width of the channel $\sigma \approx h/4\,\mu$m, but a very small amplitude. When the electric field was turned on, there was significant migration of the DNA towards the center of the channel, as quantified by the increase in σ^{-1}. The steady concentration profile, with an inverse width $\sigma^{-1} = 0.14 \pm 0.01\,\mu\text{m}^{-1}$, was obtained within 30 secs of the field being turned on. This implies a characteristic migration velocity of the order of $1\,\mu\text{m s}^{-1}$, compared with a typical convective velocity for fluid flow of around $240\,\mu\text{m s}^{-1}$ (for $Wi = 0.6$).

The velocity of a DNA molecule at the center of the channel is only weakly dependent on electric field, because its electrophoretic velocity is more or less canceled by electroosmotic flow generated by charges released from the uncoated channel walls. The electroosmotic flow is convenient in these experiments, because it reduces the convective flow of the DNA molecules without affecting the cross-stream migration (since it is a plug flow). The time scales for migration and convection then suggest that entrance effects are minimal. Any disturbance to the concentration profile at the entry to the channel would then require ~ 100 s to reach the viewing window,

whereas an upper limit of 30 s is required to focus the DNA at the center line.

When the electric field was turned off at $t = 8$ minutes, the concentration profile returned to a fully mixed state in approximately 1 minute. This is due to the convection of fresh DNA solution into the viewing window, which (in the absence of electrophoresis) takes of the order of 100 s, consistent with the observations illustrated in Fig. 6. By contrast, the relaxation of the concentration profile by diffusion would take about 3 hours, which is the timescale $h^2/4D$ for the polymer to diffuse across one half the channel ($D = 0.15\,\mu\text{m}^2\,\text{s}^{-1}$).

4.2 Characterizing the effects of shear and electric field

Steady-state measurements of the concentration distribution were obtained by flowing the DNA solution through the channel at a constant flow rate, corresponding to Weissenberg numbers $Wi = 0.3$, 0.6, 0.9, and 1.2. At each flow rate, electric fields up to 250 V/cm were applied for a total of 10 minutes for each field; 5 minutes for the concentration to come to steady state and 5 minutes for data collection. At each data point, a total of 3000 frames were averaged and analyzed as described in Sec. 3. Results for the amplitude and inverse width obtained with a standard TAE buffer solution are shown in Fig. 7.

The amplitude and inverse width show the same trend with electric field at each Weissenberg number: an increase in the extent of migration roughly proportional to $\sqrt{E}$, beginning at ≈ 5 V/cm but saturating at high fields ($E \sim 100$ V/cm) and eventually declining. There is very little migration at the lowest Weissenberg number $Wi = 0.3$, which can be understood in terms of the mechanism illustrated in Fig. 1. The polymer must be stretched and aligned towards the $\theta = 45°$ direction for there to be a significant lift generated by the coupling between shear rate and electric field; however, below the coil-stretch transition ($Wi \approx 0.5$) the polymer fluctuates around a nearly globular shape which does not generate a persistent

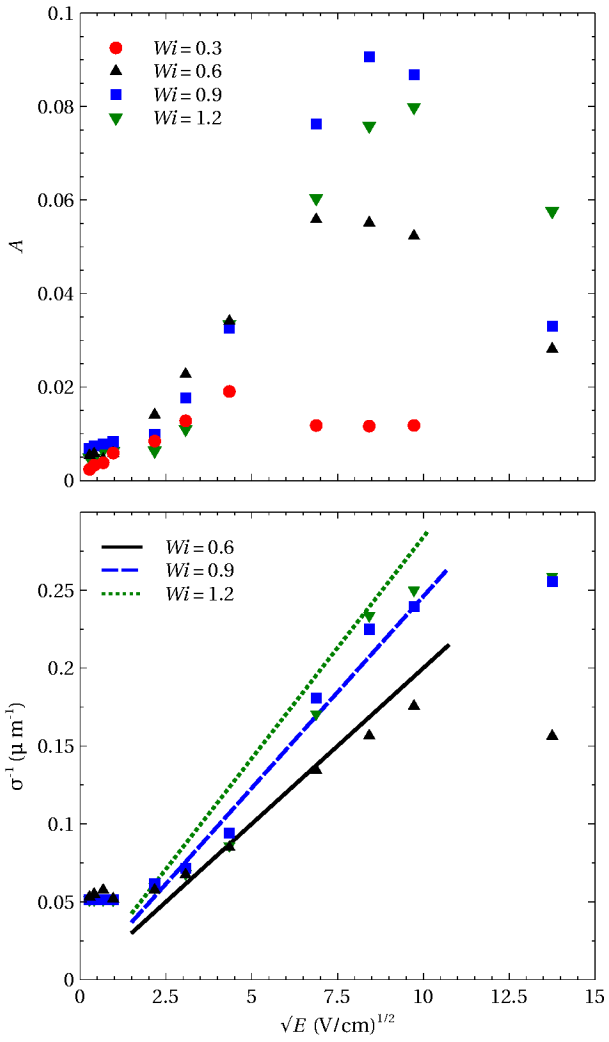

Fig. 7 Steady-state migration of DNA in a standard TAE buffer (solution S1). The effect of the electric field on the amplitude (top) and width (bottom) of the concentration profile is shown at four different Weissenberg numbers: $Wi = 0.3$ (red circles), $Wi = 0.6$ (black triangles), $Wi = 0.9$ (blue squares), and $Wi = 1.2$ (green inverted triangles). The solid lines are a fit to Eq. (2) at $Wi = 0.6$ (solid black), $Wi = 0.9$ (dashed blue), and $Wi = 1.2$ (dotted green); a proportionality constant $C = 8.9$ is used for all three Weissenberg numbers. At the lowest flow rate ($Wi = 0.3$), there is no discernible migration and the width is undetermined.

dipolar flow. The width of the concentration profile cannot be determined in this case.

At larger Weissenberg numbers we see significant migration for fields in the range of $10-200\,\mathrm{V/cm}$ as shown by the increase in the amplitude of the concentration at the centerline (top) and the reduction in its spread (bottom). For small electric fields ($E < 5\,\mathrm{V/cm}$), σ^{-1} approaches a limiting value of $0.05\,\mu\mathrm{m}^{-1}$, independent of the flow rate. The amplitude of the concentration peak is very small in this range of electric fields and we think the non-zero σ^{-1} is an artifact related to the imaging of a finite width channel; the ratio of the background signals shown in the inset to Fig. 5 has a half-width of about $20\,\mu\mathrm{m}$ as well. While we are not the first to investigate this migration experimentally[5] or to propose electrically-induced flows to account for the observations[7], these are the first experimental results that quantify the extent of migration and study its dependence on flow and electric fields.

A kinetic theory for the concentration distribution of a polyelectrolyte subjected to shear and electric fields[12] predicts that the inverse width is proportional to the product of the shear rate and electric field, $\sigma^{-1} \propto \bar{\gamma}E$, in agreement with the data in the bottom panel of Fig. 7. A fit of Eq. (2) to the experimental data, with an empirically-determined proportionality constant $C = 8.9$, is shown at the three largest Weissenberg numbers. The data follows the predicted scaling up to $Wi \approx 1$ and $E \approx 100\,\mathrm{V/cm}$. However, the theory neglects the finite extensibility of the polymer chain and so fails to capture the saturation in σ^{-1} with increasing flow rate (or Wi). In reality the polymer chain is fully extended for $Wi > 1$ and so no further enhancement of the migration is to be expected. The saturation with electric field is more complicated and will be investigated in the next section (Sec. 4.3). Nevertheless, despite the limitations at large flow rates and electric fields, the kinetic theory captures the underlying trends in the data for weak to moderate electric fields ($< 100\,\mathrm{V/cm}$), up to the limit of the coil-stretch transition.

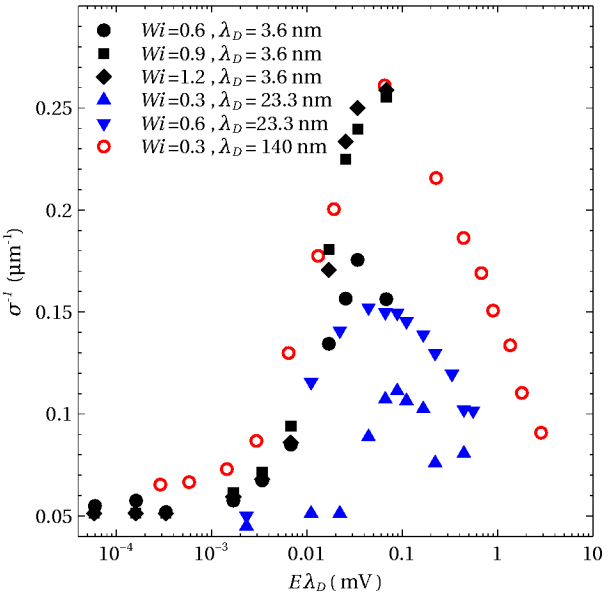

Fig. 8 Inverse width of the concentration profile as a function of electric field at different flow rates and ionic strengths. Results are shown for a standard (40 mM) TAE buffer (Solution 1: solid black symbols) and a diluted (0.4 mM) TAE buffer with 0.1 mM salt concentration (solution S2: solid blue symbols). The experiments span a range of Weissenberg numbers over the coil-stretch transition ($Wi = 0.3-0.9$). Simulations[9] at $Wi = 0.7$ and a $5\,\mu\mathrm{m}$ salt concentration ($\lambda_D = 140\,\mathrm{nm}$) are indicated by the open red circles.

4.3 Saturation and reversal

Figure 8 illustrates the saturation of inverse width with increasing electric field for different flow rates and ionic strengths (solutions S1 and S2 from Table 1). We were able to prepare stable DNA solutions in 0.4 mM TAE (diluted 100 fold from the standard solution), with the addition of 0.1 mM NaCl. The Debye length in this solution is estimated to be 23 nm, but attempts to further dilute the buffer led to a de-

crease in pH. In order to combine data from a wide range of ionic strengths ($5\,\mu$M-40 mM) we scale the electric field with the Debye length[20], $E\lambda_D$, which is the potential drop across the double layer thickness.

A saturation in the migration with increasing electric field was predicted by numerical simulations[9] that included the EIHI mechanism illustrated in Fig. 1. That prediction is confirmed by the data in Fig. 8, which show a peak value of σ^{-1} around $E\lambda_D \approx 10^{-4}$ V, independent of flow rate and ionic strength. The screening length for the reduced-strength TAE buffer (23.3 nm) is significantly larger than in the full strength buffer (3.6 nm) and there is now a measurable migration at $Wi = 0.3$, consistent with the scaling from Eq. (2).

The mechanism leading to the saturation and eventual decline of the migration remains open at this point in time. Simulations showed a rapid increase in the extension of the polymer as the electric field approached the value for maximum migration, coupled with a rotation of the major axis of the polymer toward the flow direction[9]. While these conformational changes would explain the subsequent reduction in migration, recent experiments (without flow) show that in high electric fields (around 100 V/cm) DNA molecules collapse into small entangled blobs[20], which would also eliminate the electrically induced flow fields. However, a local shear may overcome the tendency to entanglement even at high electric fields, but our present set-up cannot be used to image individual DNA molecules; this remains an area for future research.

4.4 Effect of Ionic Strength

The theory of EIHI[8] predicts that migration will diminish as the ionic strength increases (2). Experiments in a diluted TAE buffer (solutions S2-S4 in Table 1) show the expected increase in migration with increasing Debye length (solid symbols in Fig. 9), regardless of the strength of the applied field (Fig. 9). The maximum migration occurs at lower electric fields when the Debye length is reduced, consistent with the scaling in Fig. 8. At the smallest Debye length, $\lambda_D = 6$ nm, there is no observable migration. However, in the standard TAE buffer, which has an even smaller Debye length ($\lambda_D = 3.6$ nm), the migration is comparable to salt solutions with much larger screening lengths.

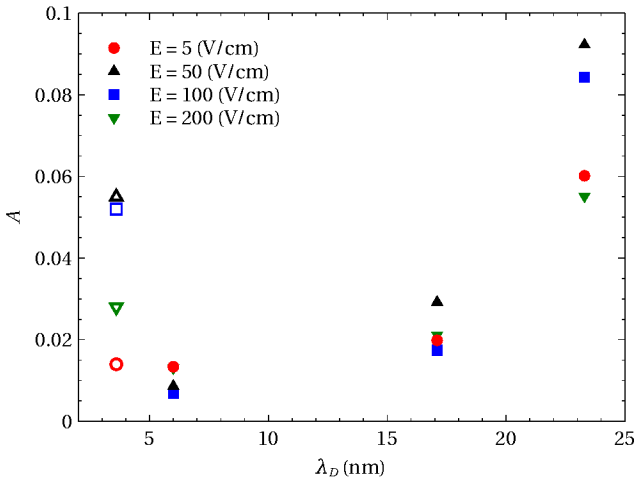

Fig. 9 Steady-state migration of DNA at various ionic strengths. Results for a diluted (0.4 mM) TAE buffer with different salt concentrations (solutions S2, S3, and S4) are shown as solid symbols; the full strength (40 mM) TAE buffer solution S1) is shown by the open symbols. Data was collected for a single Weissenberg number, $Wi = 0.6$, and a range of electric fields: 5 V/cm (red circles), 50 V/cm (black triangles), 100 V/cm (blue squares), and 200 V/cm (green inverted triangles).

The results in Fig. 9 suggest that TAE is not as effective as NaCl in screening the backbone charges, perhaps due to the size of the $Tris^+$ cations. Electrophoresis of DNA with monovalent cations has shown that the mobility is affected by an ion-specific non-equilibrium relaxation[15,21]. DNA in Na^+ buffers has a reduced electrophoretic mobility compared with

TAE buffers, which can be understood as a more efficient neutralization of backbone charges by Na^+ cations. Similarly, molecular dynamic studies on electrostatic screening of DNA also shows that smaller counterions penetrate deeper into the interior, resulting in shorter effective screening lengths[22].

5 Conclusions

We have reported the first systematic study of polyelectrolyte migration during capillary electrophoresis, which occurs when there is a concurrent pressure gradient. The extent of migration scales with electric field, shear rate, and Debye screening length as predicted by a kinetic theory of a linearly-elastic dumbbell[12], (2). However the theory fails to capture nonlinear effects that lead to saturation with increasing electric field and flow rate. Numerical simulations of a coarse-grained bead-spring model predicted a saturation in the migration with increasing electric field[9], which has been confirmed by these experiments. The peak migration occurs at a fairly consistent value of the scaled electric field, $E\lambda_D \approx 0.1\,\mathrm{mV}$, over a wide range of flow rates and ionic strengths. There is an anomaly in the migration of DNA in concentrated (40 mM) TAE buffer solutions, which is consistent with a significantly reduced screening of the backbone charges in comparison with salt solutions of similar ionic strength.

Acknowledgments

The authors thank Saif Shaikh for assistance with some of the experiments. This work was supported by the National Science Foundation (Grant No. 1067072).

References

1 J.-L. Viovy, *Rev. Mod. Phys.*, 2000, **72**, 813–872.

2 T. Shendruk, O. Hickey, G. Slater and J. Harden, *Curr. Op. Coll. Inter. Sci.*, 2012, **17**, 74 – 82.

3 R. G. Larson, *J. Rheol.*, 2005, **49**, 1–70.

4 E. S. Shaqfeh, *J. Non-Newton. Fluid*, 2005, **130**, 1 – 28.

5 J. Zheng and E. S. Yeung, *Anal. Chem.*, 2002, **74**, 4536–4547.

6 J. Zheng and E. S. Yeung, *Anal. Chem.*, 2003, **75**, 3675–3680.

7 O. B. Usta, J. E. Butler and A. J. C. Ladd, *Phys. Rev. Lett.*, 2007, **98**, 098301.

8 D. Long and A. Ajdari, *Eur. Phys. J. E*, 2001, **4**, 29–32.

9 R. Kekre, J. E. Butler and A. J. C. Ladd, *Phys. Rev. E*, 2010, **82**, 050803.

10 R. B. Bird, C. F. Curtiss, R. C. Armstrong and O. Hassager, *Dynamics of polymeric liquids. Volume 2: Kinetic Theory*, John Wiley Sons, 1987.

11 W.-C. Liao, N. Watari, S. Wang, X. Hu, R. G. Larson and L. J. Lee, *Electrophoresis*, 2010, **31**, 2813–2821.

12 J. E. Butler, O. B. Usta, R. Kekre and A. J. C. Ladd, *Phys. Fluids*, 2007, **19**, 113101.

13 R. Kekre, J. E. Butler and A. J. C. Ladd, *Phys. Rev. E*, 2010, **82**, 011802.

14 S. Gerashchenko and V. Steinberg, *Phys. Rev. E*, 2008, **78**, 040801.

15 G. S. Manning, *J. Phys. Chem.*, 1981, **85**, 1506–1515.

16 K. Günther, M. Mertig and R. Seidel, *Nucleic Acids Res.*, 2010, **38**, 6526–6532.

17 M. Arca, X. Feng, A. J. C. Ladd and J. E. Butler, *RSC Adv.*, 2014, **4**, 1083–1086.

18 J. C. Crocker, D. G. Grier *et al.*, *J. Colloid Interface Sci.*, 1996, **179**, 298–310.

19 L. Velho, A. C. Frery and J. Gomes, *Image processing for computer graphics and vision*, Springer, 2009, vol. 3191.

20 J. Tang, N. Du and P. S. Doyle, *Proc. Natl. Acad. Sci. U. S. A.*, 2011, **108**, 16153–16158.

21 E. Stellwagen and N. C. Stellwagen, *Biophysical journal*, 2003, **84**, 1855–1866.

22 A. Savelyev and G. A. Papoian, *J. Am. Chem. Soc.*, 2006, **128**, 14506–14518.